AIAA SciTech Forum
11–15 & 19–21 January 2021, VIRTUAL EVENT
AIAA Scitech 2021 Forum

10.2514/6.2021-1301

On the use of liquid nitrogen droplets as flow tracers in cryogenic flow facilities at NASA Langley Research Center

Jonathan E. Retter[1] and Ross A. Burns[2]
National Institute of Aerospace, Hampton, VA, 23666, United States

Jordan M. Fisher[3]
Purdue University, West Lafayette, IN, 47906, United States

Josef J. Felver[4]
Spectral Energies, LLC, Dayton, OH, 45430, United States

Daniel T. Reese[5] and Paul M. Danehy[6]
NASA Langley Research Center, Hampton, VA, 23681, United States

The injection of liquid nitrogen droplets to cool the gas temperature in cryogenic wind tunnels is discussed as a method of *natural* seeding for velocimetry-focused, particle-based, laser diagnostics. Historical observations and issues with seeding are presented for both ground-test facilities of interest in this work at NASA Langley: the 0.3-m Transonic Cryogenic Wind Tunnel (TCT) and the National Transonic Facility (NTF). Recent observations of natural seeding with a Rayleigh scattering instrument are presented in the two facilities, which motivated the purposeful use of a pulse-burst laser system to observe the particles directly with a sequentially operated laser sheet for the first time. Time-resolved image sequences of unevaporated liquid nitrogen droplets were readily acquired for tunnel total temperatures of 200 K and below. The preliminary results promote a discussion on the fitness of these natural particles as flow tracers for either a particle image velocimetry or a particle tracking velocimetry instrument in these high-Reynolds-number facilities.

I. Nomenclature

f	=	lens focal length (mm)
LN_2	=	liquid nitrogen
M	=	Mach number
PIV	=	Particle Image Velocimetry
PTV	=	Particle Tracking Velocimetry
P_t	=	Total pressure (psia)
Re	=	Reynolds number
T_t	=	Total temperature (K)

[1] Research Engineer, AIAA Member
[2] Research Engineer
[3] Graduate Research Assistant, AIAA Student Member
[4] Formerly a Research Scientist, Currently a Physicist at the Air Force Research Laboratories, AIAA Member
[5] Research Engineer, AIAA Member
[6] Senior Technologist, AIAA Associate Fellow

II. Introduction

Cryogenic wind tunnels remain the only ground-test facilities that produce accurate Reynold number (*Re*) testing at flight relevant Mach numbers (*M*) for geometrically-similar test models [1,2]. The two large-scale continuous-flow facilities in the world that accomplish these conditions are the European Wind Tunnel (EWT) [3] in Cologne, Germany and the National Transonic Facility (NTF) [4] at the NASA Langley Research Center. Higher *Re*'s are achieved by lowering the gas temperature and increasing the pressure to increase the gas density and lower the viscosity. Liquid nitrogen droplets are injected into the closed-circuit tunnel which evaporate and lower the gas temperature. To avoid issues with water vapor freezing in the facility and causing damage to the tunnel or model, the tunnel is purged before every run, ideally leaving the remaining gas as pure nitrogen. While these tunnels are quite unique in infrastructure and capability, they do provide numerous challenges with the implementation of non-intrusive optical diagnostics to measure off-body flow properties.

At NASA Langley, the pilot facility for the NTF is the 0.3-m Transonic Cryogenic Wind Tunnel (TCT) [5,6]. As described in the references below, this facility has been used since its inception to demonstrate the applicability of measurement techniques in these harsh environments before implementing them in the NTF. A recent example of such a transition is with the molecular tagging technique denoted as Femtosecond laser electronic excitation tagging (FLEET) [7]. With FLEET, a detector views the emission from elevated energy levels of nitrogen as it moves with the flow, making it a useful technique for pure nitrogen facilities. FLEET has shown many promising results in the 0.3-m TCT [8–13] and has now been implemented in the NTF [14,15]. While useful as a research tool, the limited size of the measurement volume inherently limits the scalability of the technique and for now remains a one-component velocity measurement along a one-dimensional line, requiring significant time to move the measurement position around to map out any large-scale flow features in an engineering setting. Furthermore, in this large facility it is difficult to focus the FLEET line to a point as has been done in past works [8,16] so that only a single component can be measured in NTF with a single detector. Therefore, it is of interest to expand to larger field-of-view techniques such as Doppler global velocimetry (DGV), particle image velocimetry (PIV), or particle tracking velocimetry (PTV) applied over a large laser sheet in two-dimensions. Furthermore, using a single-camera FLEET or DGV instrument in the NTF would only measure one velocity component while PIV and PTV have the advantage of measuring two components with a single camera.

However, DGV, PIV and PTV require seeding of the flow with small tracer particles to measure the particle velocity and relate it back to the actual flow velocity. Fortuitously, an inherent feature of these cryogenic facilities is the presence of natural seeding in the flow. These "natural seeds" may be from residual water vapor, un-evaporated LN_2, oil leaks, particulates, or residual carbon dioxide in the nitrogen supply, and occur intermittently. Researchers at the EWT deemed this natural seeding "*insufficient to reliably establish planar velocimetry techniques*" and instead demonstrated success with *active* seeding by adding water vapor to the flow that turns to ice crystals under cryogenic conditions for DGV [17] and now PIV [18–22]. Unfortunately, such a seeding method is not permitted in the NTF due to issues in the past with frost occurring on the models from water vapor in the tunnel, bringing into question the quality of the measured data during these tests [23]. Internal tunnel insulation absorbs residual water vapor, forcing tunnel procedures to constantly mitigate the humidity in the tunnel and strongly discourage the purposeful addition of water vapor. These requirements necessitate an alternative method of "clean seeding" [24] or use of what naturally exists in the flow. However, with the implementation of new, high-power pulsed-laser systems along with increased detector sensitivity, we plan to again explore natural seeding in hopes of identifying tunnel operating conditions to develop a reliable PIV or PTV instrument and expand the current off-body velocity measurements to two-dimensions.

The selection and quality of the chosen seed particle is critical in order to accurately measure the instantaneous flow of the medium of interest [25]. Unfortunately, little information about LN_2 droplets for velocimetry are reported in literature. There are reports on the condensation of LN_2 aimed at the use in cryogenic facilities [26], where most are NASA Technical Memorandums from the development of the 0.3-m TCT [5,27–30]. Characterization studies of cryogenic fluid sprays have examined droplet sizes and velocities for dermatology [31,32] and spacecraft propulsion [33–36] purposes, using the droplets as flow tracers via commercial optical sizing and velocity instruments and small-scale laser techniques, respectively. However, in those studies the droplet velocity was the quantity of interest, therefore it remains unclear whether or not injected droplets will adequately trace an external flowfield.

At risk of pursuing such a seed source that does not adequately follow the flow, the abundance of observed LN_2 droplets from previous studies encourages us to at least examine the possibility to gain any useful off-body flow velocity information. There are numerous examples of velocity studies utilizing a source of seeding that naturally occurs in the test medium, including large-scale atmospheric or environmental flow studies [37–42], in-flight PIV measurements [43], biomedical applications [44,45], and in several wind tunnel facilities [46–50]. As is inherent to any natural seeding technique, there is limited-to-no control over the density and size distribution of the particles in

the flow, which may encourage the use of PTV trajectory algorithms over PIV cross-correlation algorithms and will remain an ongoing topic of discussion with this work. In addition, the ability of a natural seed to follow the flow is of question, as shown by the lag of natural sand particles in an appropriately seeded cross flow with simultaneous PTV/PIV in Zhang et al. [51].

The goal of this work is mainly to review the use of and our observation of natural and/or active seeding in the NASA Langley cryogenic wind tunnel facilities. We will discuss (1) the existing literature relating to seeding the facilities, (2) present recent, unpublished LN_2 droplet observations with Rayleigh scattering instruments used to (3) motivate a devoted effort of particle velocimetry at the 0.3-m TCT. The discussion is divided by facility, beginning with the 0.3-m TCT.

III. The 0.3-m Transonic Cryogenic Wind Tunnel

The major assumption in the phased approach of this study is that the two cryogenic facilities, 0.3-m TCT and the NTF, both have similar infrastructure and the observations from one may infer behavior in the other (e.g. any natural seeding existing in the pilot facility should also be present in the NTF). While similar, the infrastructure of the NTF in comparison to the 0.3-m TCT are clearly not the same, and this assumption remains a challenge . However, in the pursuit of other diagnostic techniques, our group has observed natural seeding in both facilities, providing preliminary confidence to move forward. This section includes a brief discussion of the 0.3-m TCT layout, an overview of the history of seeding in the facility, and a discussion of LN_2 observations from previously unpublished Rayleigh scattering measurements.

A. 0.3-m TCT Layout

The relative locations of the test section and the LN_2 injection in the 0.3-m TCT are shown in Fig 1. The tunnel is closed-loop and oriented vertically, with the view in Fig. 1 from what is known as the "near side" of the facility. The LN_2 is injected just downstream of the test section, passes through the fan, past the nominally gaseous nitrogen exhaust (GN2), through anti-turbulence screens, and finally into the test section. The total path length a LN_2 droplet must travel to reach the test section is ~20-m. Under design conditions, all injected LN_2 should evaporate before reaching the test section to avoid acquiring any aerodynamic data in a two-phase flow. The original injection design is found in Kilgore [52], although various combinations of injectors have been used through the years. Three 40-mesh anti-turbulence screens (i.e. nominal openings of 420-μm) are present before the 10.7:1 contraction into the test section [53]. The current iteration of the test section has a 0.33-m by 0.33-m cross section with fixed side walls and top and bottom flexible walls with optical access only available from the sides of the test section. Earlier iterations of the test section included a 3-dimensional octagonal cross section followed by a 2-dimensional slotted test section, but the flex walls were installed in 1985 [53]. Note that the test-section geometry is a major difference between this facility and the NTF, as the NTF has a slotted test section.

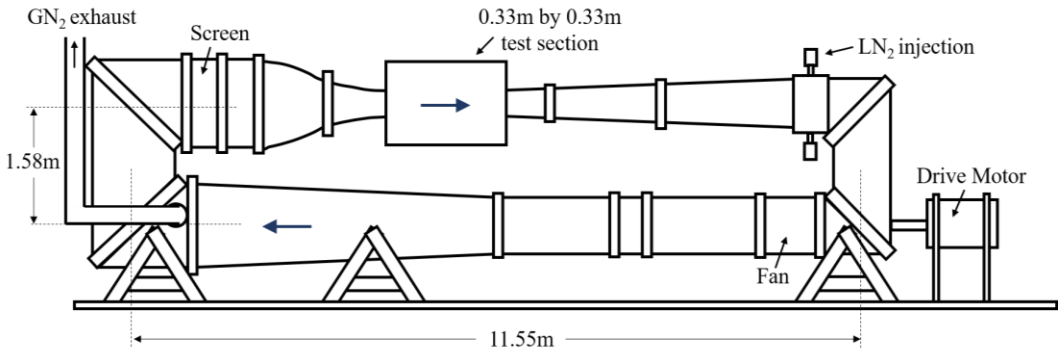

Fig. 1 0.3-m TCT layout from the near side of the facility recreated from [53].

B. Early Observation and Use of Seeding in the 0.3-m TCT

After coming online in 1973, an early focus on LN_2 droplets in the 0.3-m TCT was with respect to setting the usable tunnel temperature limits of the facility. The goal of the facility is to maximize the *Re* while maintaining a singular gas-phase environment. The lower the temperature the facility operates, the higher the density and higher the *Re*, but also the closer one is to the condensation limit of nitrogen and the onset of LN_2 droplets forming in the flow. This "condensation boundary" has different theoretical total temperature, T_t, limits depending on the local *M* as the

local static temperature will decrease with increasing M for a fixed T_t. Therefore, when operating the facility at a T_t based on the reservoir limit (i.e. $M = 0$), *local* condensation may occur in regions of the flow with higher M and thus lower static temperatures, such as in the test section freestream or near a model surface.

The first measure of this condensation limit was reported in 1978 with a series of pitot probes mounted off the floor of the test section in the streamwise direction with the goal of measuring the drop in pressure coefficient as a function of flow position in the test section [28]. Any drop in total pressure is due to the rise in temperature from the latent heat of condensation of gaseous nitrogen. Results showed the condensation limit occurred at temperatures slightly below the freestream saturation temperature but above the reservoir saturation limit. The drop in pressure increased with distance down the test section, suggesting an increase in LN_2 droplets as the flow proceeds through the test section. In addition, the onset of condensation ~3 K below the freestream saturation limit suggests the heterogeneous nucleation of LN_2 droplets – perhaps seeded by unevaporated droplets from the LN_2 injection. As a follow-up study to examine local effects of condensation, a NACA 0012-64 airfoil model was placed in the test section with pressure ports located chordwise on the upper surface to again view the drop in pressure, only now on the surface of the airfoil where even higher local M's are expected [29]. However, once again the onset of condensation appears to correlate more with the freestream saturation limit and not the local limit above the airfoil model. The onset of condensation appeared to occur over the entire airfoil at the same T_t, once again suggesting heterogeneous nucleation of droplets in the freestream from existing particles as opposed to homogeneous nucleation from the gas phase.

Shortly after the observation of these naturally occurring droplets, a laser doppler velocimetry (LDV) instrument was applied to the freestream flow in the 0.3-m TCT in 1981, utilizing what was assumed to be the unevaporated LN_2 droplets reaching the test section as the flow tracer [54]. Excellent agreement with facility velocity measurements was achieved from T_t = 100 to 250 K across a range of M = 0.20 to 0.77. Even with a point measurement device, a significant number of particles (10-20 per second) was observed for all conditions. While no direct particle size measurements were recorded in this study, based on the large distribution in scattered signal intensity, the physical size distribution of the droplets was likewise suspected to be large. However, the measured velocity standard deviation was low, suggesting a negligible velocity dependence on droplet size for this freestream flow.

A second velocity measurement instrument, known as a laser transit anemometer (LTA), was also applied in the 0.3-m TCT over the top surface of a NACA 0012 airfoil in 1982 [55]. This technique utilized two focused laser beams at known distances from one another, where a particle (or LN_2 droplet) immersed in the flow scattered off the first and then second beam, generating two distinct scattered signals on the first and second photomultiplier tubes (PMTs) at known times. Therefore, velocity and flow angle can be determined from the time of the scattered spikes and the physical position of the two laser foci. Measurements over the full range of tunnel conditions were performed (T_t = 95 to 285 K, M = 0.11 to 0.85), where once again the natural seeding present in the facility was used as the flow tracer. The measured velocity drop across a normal shock over the top surface of an airfoil was within 5% of theory – an incredible demonstration of accuracy with these uncharacterized tracer particles.

The use and abundance of the 0.3-m TCT natural seeding quickly led to efforts to better characterize these seed particles. The first was an effort in 1982 to determine the phase of the particles (i.e. liquid droplets or solid particles) by means of a hot-wire probe in the freestream of the test section [56]. The measurable was the positive-going or negative-going voltage pulse of the hot-wire when struck by a seed particle in the flow. If these seeds are liquid, they would stick to the wire and cool it, causing a positive voltage spike. However, a solid particle would strike the wire and scatter off, temporarily stressing the wiring, increasing the temperature and producing a negative voltage spike. Nearly all voltage spikes measured were positive going, suggesting the seed particles were LN_2 droplets. However, this study was only performed at total temperatures surrounding the saturation limit from 79.4 to 105 K, likely predetermining the source of the measured particles to be LN_2 droplets condensing from the freestream.

A follow-up study in 1984 utilized an optical particle sizing instrument to determine the size of the particles in the flow by collecting light scatter at 90 degrees onto a PMT [30]. Measurements were performed in the settling chamber and downstream of the fan. Throughout the tests, a peak particle diameter of 3 μm was recorded and was attributed to oil droplets, since these were seen when the tunnel warmed up to 200 K. A large distribution of larger diameter particles was observed and postulated to be from LN_2 droplets due to the proximity in time to an event where a large amount of LN_2 was added to the facility. Such events included when the operator purposefully injected more LN_2 than what was required, or when the tunnel was "on point" after dropping from a higher temperature.

By defining oil droplets as the main source of natural seeding, this optical particle sizing instrument brings into question the earlier assumption that the tracer particles were LN_2 droplets. Perhaps it had been oil the entire time, because when the LTA instrument was reintroduced to the facility in 1985 after finding and fixing an oil leak, no appreciable natural seeding was present in the facility [57]. Pulsing the LN_2 injection did produce particles, but not enough for steady-state operation, so air was injected into the tunnel and the residual moisture froze and produced plenty of ice crystals (3000 particles/sec), but the injection rate was minimized to prevent frost on the cylinder model

used in the study yielding fewer ice crystals (100 particles/sec). Flow angle and velocity measurements were then performed in the wake of a circular cylinder using LTA at T_t = 225 K and M = 0.3.

The last published study on the use of natural seeding in 0.3-m TCT was from 1986, where the tunnel was purposefully operated at temperatures at or near the condensation limit of the tunnel (83-101 K) to produce large quantities of LN_2 droplets in the test section to illuminate with a laser sheet for flow visualization over a delta wing [58]. This study was performed before the installation of the flexible top and bottom tunnel walls, and therefore had optical access from above, allowing a Helium-Neon laser to form a sheet nearly perpendicular to the imaging system from the side walls. However, operation at these conditions led to concerns of *local condensing* of LN_2 in the vortex over the delta wing, as the high-velocity core of the vortex was unexpectedly well seeded.

An informative summary of the test techniques used in 0.3-m TCT was released in 1986, including most of the previously mentioned studies and, almost more importantly, notes on unsuccessful techniques as well [59]. A discussion of the use of LN_2 droplets is included (operation near condensation limit, pulsing the injectors to generate a temporary cloud of particles), as well as the forms of active seeding such as lubricating oil leaks, ice crystals from air, and Kaolin powders for solid particle seeding. Both the oil and ice crystals were believed to cause model leading-edge erosion and were not recommended for further use. The kaolin powder along with the oil required extensive cleanup after use and was also discouraged from future use. The authors summarized the velocimetry review by stating an adequate method of seeding currently does not exist – a thought that remains true today.

Succeeding this review, there is a significant gap in literature on the use of laser diagnostics in 0.3-m TCT. Not until the coupled works from 1999 and 2002 on the implementation of Rayleigh scattering do these laser-based measurement techniques return [60,61]. While there is no explicit mention of LN_2 droplets in the flow, personal communications with the authors revealed a large number of droplets when the facility changes conditions. A wait time of several minutes was required for the droplets to evaporate before using a technique such as Rayleigh scattering which is contaminated by any Mie scattering from the droplets.

C. Recent Rayleigh Scattering Observations

Noting the issues with seeding these cryogenic facilities in the past along with the introduction of a seed-free molecular tagging instrument specific to nitrogen (FLEET), our group began a devoted effort to apply this technique (and variations on it) in the 0.3-m TCT [8–10,12,13,62]. Above atmospheric pressure the FLEET signal increases with gas density and therefore appears to be a promising measurement technique in transonic cryogenic facilities which operate at low temperatures and high pressures. With a FLEET instrument, by simply removing the spectral filter and gating the detector on the arrival of the laser pulse, one gets a Rayleigh signal in a sense for “free”, as was taken advantage of to fully characterize the use of such a technique in this flow facility for density measurements [63]. Unpublished in those results however, are once again the observation of LN_2 droplets in the facility. A brief discussion of these observations, along with visualization of three tests cases are presented here. The optical setup and specific experimental details are found elsewhere [63].

Liquid nitrogen droplets were readily seen in the facility under cryogenic conditions, although the number of droplets varied significantly depending on the conditions of the tunnel. Three staged cases were studied to identify the cause and effect of the LN_2 number density for a flow at M = 0.4: (1) a fast drop in pressure, (2) a fast rise in pressure, and (3) a slow, incremental drop in pressure over time. All three cases are detailed in the three rows of Fig. 2, where the columns represent the tunnel conditions (a-c), the measured droplet count (d-f), and an example single image of the Rayleigh scattering signal (g-i). The tunnel conditions are recorded at 20 Hz, while the electron-multiplying charge-coupled device (EMCCD) acquired Rayleigh images at roughly 5 Hz (exact frame rate is unknown) but was not synced with the tunnel acquisition system. Due to the uncertainty in the detector acquisition rate and the absolute timing with respect to the tunnel conditions, the domain of Fig. 2d-2f is left as an approximate time (i.e. ‘~time (s)’). However, the Rayleigh acquisition encompassed the tunnel event of interest, providing confidence we are seeing the resulting unevaporated LN_2 concentration in the test section following the given event. A droplet counting tool developed for this work transformed the raw images to binary images based on a threshold intensity and simply counted every unconnected pixel grouping as a single droplet.

The first example of a pressure drop from 54 to 36 psia, occurring over a total time of ~70 s, is seen in Fig. 2a. A drop in tunnel pressure is accomplished by opening the GN_2 exhaust valve to relieve existing pressure in the facility to the atmosphere as seen earlier in Fig. 1. The initial pressure drop overshoots in the first 16 s to ~33 psia, followed by a gradual rise to the setpoint of 36 psia. The facility temperature is positively correlated to the pressure over this period of time, where a drop in pressure leads to a small drop in temperature from 123 to 119 K, followed by the rise in both variables to the set point. We believe it is this small drop in temperature when the facility control loop continues to inject LN_2 over the first 14 s of the pressure drop before the controller steps in to stabilize the temperature that leads to a sudden rise in the droplet count in the test section seen in Fig. 2d. This correlated behavior of pressure and

temperature during a pressure drop was seen and modeled with the initial installation of the 0.3-m control system (see Figs. 2-3 in [64]), likely due to the "*lag corresponding to the transit time from the injection valves to the screen section where temperature is measured*" [64]. An example single-shot Rayleigh image for the moment in time marked in red in Fig. 2d is displayed in Fig 2g. After the initial rise in LN_2 concentration, there remains a steady-state value of droplets when the tunnel returns to conditions considered to be "on point", or within procedural bounds on the tunnel properties.

However, a pressure rise of the facility, seen in Fig. 2b, occurs more slowly and is not correlated with the facility temperature and leads to no change in the observed LN_2 concentration over the course of the rise (Fig. 2e). Only occasional droplets are observed, and the Rayleigh images are predominantly molecular scattering (Fig. 2h).

Finally, incremental 1 psia drops in facility pressure appear correlated with ~0.3 K drops in temperature as seen in Fig. 2c. While minuscule, these temperature drops roughly equate to pulsing the LN_2 injectors for each incremental change in P_t, therefore leading to a near continuous concentration of LN_2 droplets in time above the typical baseline level (i.e. compare Fig. 2f to 2e). An example single Rayleigh image is seen in Fig. 2i.

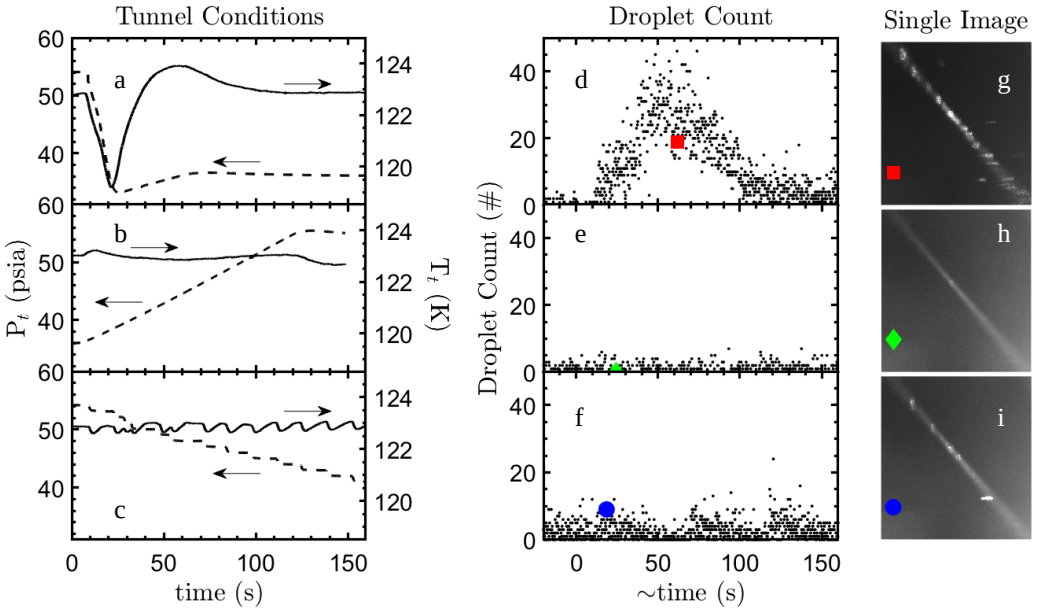

Fig. 2 0.3-m TCT flow properties as a function of time, seen as (a-c) the facility properties, (d-f) the LN_2 concentration over a fixed volume determined from (g-i) single-shot Rayleigh scattering images. The first row denotes a fast pressure drop (a, d, g), the second row shows a pressure rise (b, e, h) and the last row shows incremental drops in pressure (c, f, i). Note that the x-axis for (d-f) is left as an approximate time ('~time') due to the uncertainty in both the detector frame rate and the absolute timing with respect to the acquisition of the tunnel conditions.

While specific to one total temperature range of the facility, these observations demonstrate the ability to *actively* produce *natural* seeding by routine changes to the tunnel conditions. The case of most interest is the fast drop in pressure, as enough droplets remain in the test section for several minutes once the tunnel returns to on-point conditions typical of actual data acquisition used to collect aerodynamic measurements. Incremental drops in pressure prevent the facility from ever being on-point, and while it remains useful from a diagnostic perspective, it's not as interesting from an aerodynamic perspective as the *Re* of the facility is constantly changing. These observations alone prompted the devoted particle imaging effort described in Section V.

IV. The National Transonic Facility

The success of the 0.3-m TCT led to the development of the much larger National Transonic Facility next-door, becoming the premier high-*Re* test facility in the US. Besides the physical scale, numerous details differ between the two, such as the injector geometry, the size (4.2-mm spacing) and number (4) of the anti-turbulence screens [65], and the contraction ratio (the NTF is 14.95:1), however the injection of LN_2 to cool the flow remains similar. Therefore, our desire to use this form of natural seeding remains for the NTF as well. In 1982, two years before the NTF was brought online, there was a documented need for off-body velocimetry methods in the facility [66] – a feat which was

not accomplished until the addition of FLEET in 2019 about 37 years later and 35 years after the NTF first operated [14]. In comparison to the 0.3-m TCT, there is a noticeable lack of literature relating to the existence of LN_2 droplets in the facility, but once again thanks to recent published [67] and unpublished Rayleigh scattering measurements, we've noticed significant droplets/particles present in the NTF test section, encouraging the future use of a PTV or PIV instrument.

A. The NTF Layout

A top-view layout of the NTF is shown in Fig. 3 with an insert of the 0.3-m TCT to scale in the low-speed diffuser. While the components are similar to the 0.3-m TCT, the physical scale is much larger, as now for the same flow conditions a LN_2 droplet must travel ~120-m from the injection to the test section as opposed to only ~20-m in 0.3-m TCT. The scale of the facility also provides numerous issues with optical diagnostics, as the detectors and optics must be housed in environmental controlled containers within the plenum and are inaccessible during testing, requiring remote operation of all components [14]. Simple troubleshooting of equipment and optical alignment that would otherwise take hours may require several weeks or even months until the test is complete, and air is returned to the test section such that one can physically reach the equipment. Another notable difference is the test section, as the NTF test section is slotted, where flow can escape to the surrounding plenum for pressure relief while the 0.3-m TCT has solid, flexible walls.

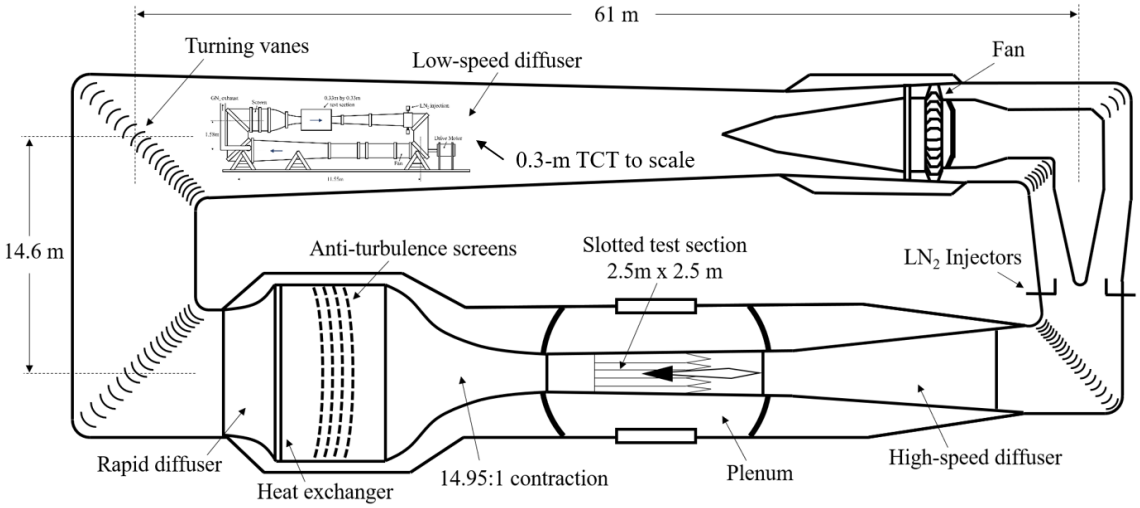

Fig. 3 Top view of the NTF adapted from [4]. An inset of the 0.3-m TCT layout is shown to scale within the low-speed diffuser.

B. Early Observation and Use of Seeding in the NTF

Literature contains only a few examples of seed particles in the NTF. As mentioned previously, injecting water vapor that would then freeze under cryogenic operation to produce ice crystal seeding was never an option in the NTF as it is in the EWT, because instead of evaporating, the residual water is absorbed by insulation internal to the tunnel circuit in the low-speed diffuser when the tunnel warms up. Therefore, the moisture returns to the circuit from the insulation in later tests and can freeze on model surfaces [23]. Water vapor will continue to not be an option unless a change in the insulation infrastructure is made. Furthermore, unpublished plans in the 2000's to use alcohol were proposed but abandoned for safety reasons, and CO_2 seeding was attempted but provided particles over a very limited range of operating conditions, and therefore the tunnel remains without an active seeding method.

However, significant natural seeding is present in the NTF and was observed indirectly in 2010 when examining the laminar-to-turbulent transition over a wing model with temperature sensitive paint [68]. For a fixed flow condition, the turbulent-wedge positions on the leading edge of the wing changed with time, leading the authors to conclude "*the loss of laminar flow is likely the result of frost or oil on the leading edge"*, which are both forms of natural seeding in the facility.

A more direct observation of particles developed from what was meant to be a Rayleigh scattering study in the NTF by Herring *et al.* in 2015 but quickly became a report on the observation of natural seeding over a variety of flow conditions [67]. The authors speculated the particles were from dust or pieces of the internal insulation, since particles were seen in air mode and cryogenic mode. Continuous observations of particles in air mode are unique to the NTF and were observed to increase with a temperature increase from 322 to 327 K. In the 0.3-m TCT operated in air mode particles – likely from residual dust in the facility – are observed during the first minute of operation after the tunnel is closed up but not thereafter. In nitrogen mode, unevaporated LN_2 droplets were not specifically mentioned as sources of the natural seeding, but the authors noted the observed particle count increased under cryogenic conditions, and therefore LN_2 droplets might be the culprit. Another unique feature of the NTF is the sudden increase in particle concentration when the flow is turned off, possibly due to particles passing through the slotted test section and being stored in the plenum and returning to the test section once the flow stops. While not useful for flow diagnostics, this facet is not true of the solid-walled 0.3-m TCT, and unfortunately may lower the particle concentration from what a solid-wall equivalent would offer.

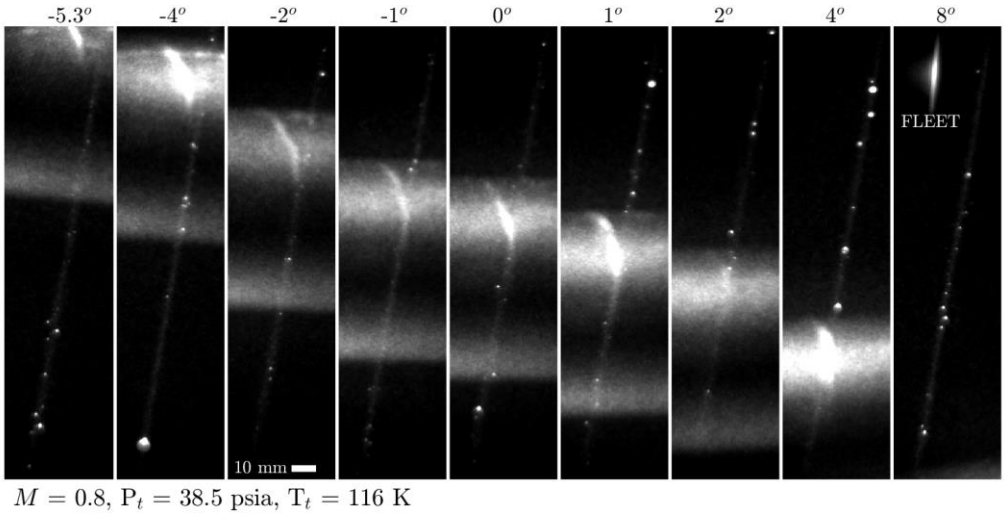

Fig. 4 Single-shot Rayleigh scattering images in the wake of a flow in the NTF for pitch angles of -5.3° to 8° with an insert of an average FLEET signal from 341 laser shots in the upper right corner of the figure.

C. Recent Rayleigh Scattering Observations

With the recent installation of a FLEET instrument in the NTF by Reese *et al.* [14], simply viewing the Rayleigh scattered signal by overlapping the detector exposure with the incident laser pulse also allows one to view any Mie scattering from natural particles in the flow. Examples of Mie scattering for single laser shots over the course of a pitching angle sweep of a model in the NTF are shown in Fig. 4 for flow conditions of M = 0.8, P_t = 38.5 psia, and T_t = 116 K, where appreciable levels of presumably LN_2 droplets are present in the focused beam. The sting is clearly visible for each pitch angle and presents a well-known problem of laser scattering when viewing signals at the laser's frequency. Each image was recorded while the facility was acquiring aerodynamic data (i.e. the facility was "on-point"), and thus represents a typical flow environment for these conditions. For spatial comparison, an average FLEET image from previous measurements [15] is overlaid (on the same physical scale) on the upper right portion of Fig. 4.

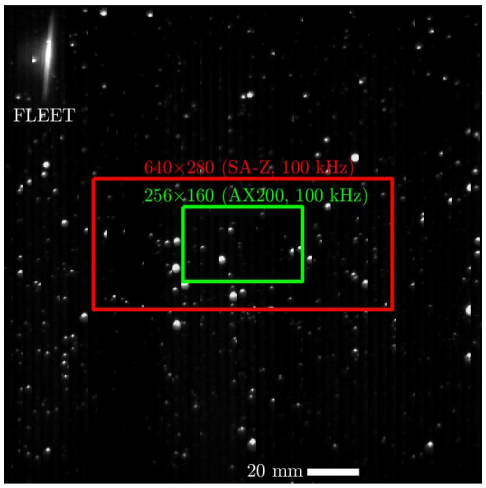

Fig. 5 Example full detector image pieced together with individual Rayleigh scattering images with an overlaid average FLEET image to scale. Representative pixel sizes for two detectors are shown for acquisition at 100 kHz.

To better visualize a best-case example of the seeding density with the introduction of a high-power laser sheet as opposed to a focused point, we can piece together single-shot Rayleigh scattering images of the particles to fill the pixel size of the 1024x1024 detector used in the NTF, generating a synthetic seeding image in Fig. 5. Assuming these conditions are repeatable, there is clearly adequate seeding covering the entire image, promoting the ability to measure velocity over the entirety of the detector. However, in practice we would prefer to utilize a pulse-burst laser system to generate time-resolved datasets which will necessitate a smaller field-of-view due to the increased frame rate required of the detector to match the high repetition rate of the laser. For the detector used in this study, a Photron AX200, a full 1024x1024 readout is only allowed up to 6.4 kHz, whereas a more realistic framerate for this flow would be 100 kHz resulting in a decrement of the available screen size to 256x160 pixels. The Photron SA-Z, another high-speed imaging system available in our lab, would have a slightly improved field-of-view at 640x280. These reduced fields-of-view, shown in Fig. 5, limit the gains one would achieve over a FLEET instrument by using these detectors for time-resolved imaging. Using a shorter focal length lens to increase the field-of-view or even switching to pulse-pair PIV (which could utilize the full field-of-view) as opposed to time-resolved measurements are both solutions to increase the field-of-view. Regardless, clearly there are LN_2 droplets in the NTF, and their usefulness for now remains unknown but promising. Potential issues that require further investigation include the droplet size and corresponding lag from the gaseous flow. Furthermore, additional studies, similar to those performed in the 0.3-m TCT, are required to characterize the conditions over which the droplets occur.

V. 0.3-m TCT Particle Imaging Setup

With the historical and recent observations of natural seeding in the 0.3-m TCT and the NTF, we have now purposefully set out to determine the fitness of these particles as the seed source for a planar velocity imaging instrument. Depending on the seed concentration, either a PIV cross-correlation algorithm or a PTV particle tracking algorithm can infer the particle velocity and help improve our understanding of the off-body flow velocity in engineering environments. The new optical assembly, initial results, and remaining questions and concerns are discussed in this section.

A. Optical Setup

The particle imaging instrument included a Spectral Energies QuasiModo pulse-burst laser (10 ns pulse duration, 100 kHz burst for 10 ms, 532 nm) to illuminate the flow and a Photron SA-Z synchronized to the laser burst to image the particles. At 100 kHz, the detector field-of-view decreases to 640x280. With a focal length lens of f = 180 mm at f/8, the total physical field-of-view was roughly 56x25 mm, with only ~6.6 mm of the vertical plane of that being in focus due to imaging the laser sheet at an angle.

The facility only has optical access from the sides and requires imaging through a plenum section that shares the cryogenic temperatures and elevated pressure of the flow. A schematic of the experimental setup is shown in Fig. 6a. A more detailed version of the test section is found elsewhere [8]. An imaging periscope mounted in the plenum allows the camera to look down on the laser sheet, which passes through the imaging window at an angle to avoid front- or back-surface reflections of the windows in the camera field-of-view. Sheet-forming optics include an f = -80-mm cylindrical lens collimated by an f = 300-mm spherical lens to form a focused ~50-mm wide laser sheet in the center of the

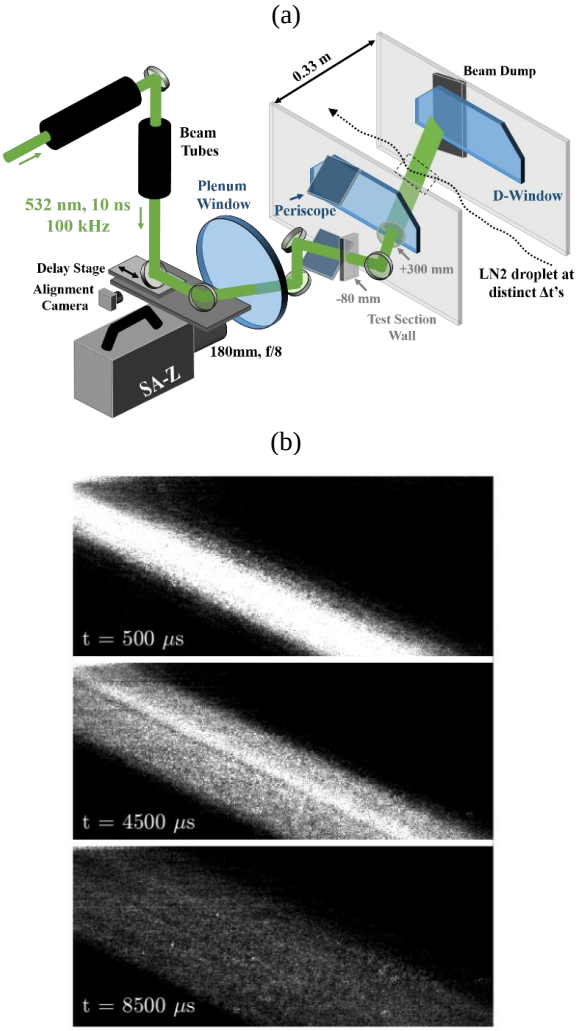

Fig. 6 (a) Experimental setup and (b) the change in laser sheet width through a burst as seen from the Mie scattering of LN_2 droplets.

test section. In practice, the beam profile from the pulse-burst system changed in time, causing the sheet width to change within the burst as seen in Fig. 6b. Future attempts with relay imaging the beam from the source or rotating the beam axis by 90 degrees may improve the performance within a burst. Nonetheless, data presented below typically used images acquired late in the pulse when the laser sheet was more uniform and wider.

As the tunnel cools under cryogenic conditions, the thermal contraction of the facility changes the position of the incoming laser beam on the turning mirrors. To account for these changes, a small alignment camera views the reflection of the CW alignment laser from the pulse burst system off the plenum window and turning mirrors inside the plenum. Any deviation was corrected with motorized stages and mirror mounts located on the two turning mirrors before the plenum window. The outside of the plenum window requires a nitrogen purge to prevent residual water vapor in air from freezing on the window surface. Unfortunately, the purge ring failed (became clogged, restricting the purge flowrate) on our initial tests, limiting the results down to T_t = 160 K. Nonetheless, encouraging results were obtained over a range of operating conditions.

B. Observation of Naturally Occurring Particles

In air mode, only a few particles are observed in the first few minutes of tunnel operation and are therefore not useful as a seed source. These particles are likely dust or pollen in the tunnel that accumulated while the tunnel was off. However, while the tunnel is filling with nitrogen to purge out the air in preparation for operation in cryogenic mode, significant levels of particles are observed through the purge. A purge entails the tunnel operating at T_t = 270 K, with three pressure cycles from P_t = 30 to 18 psia at M = 0.3, where ideally the injected nitrogen evaporates and fully replaces the existing air in the tunnel. Particles seen during the purge are likely from residual frozen water vapor from the air and LN_2 droplets from the injection.

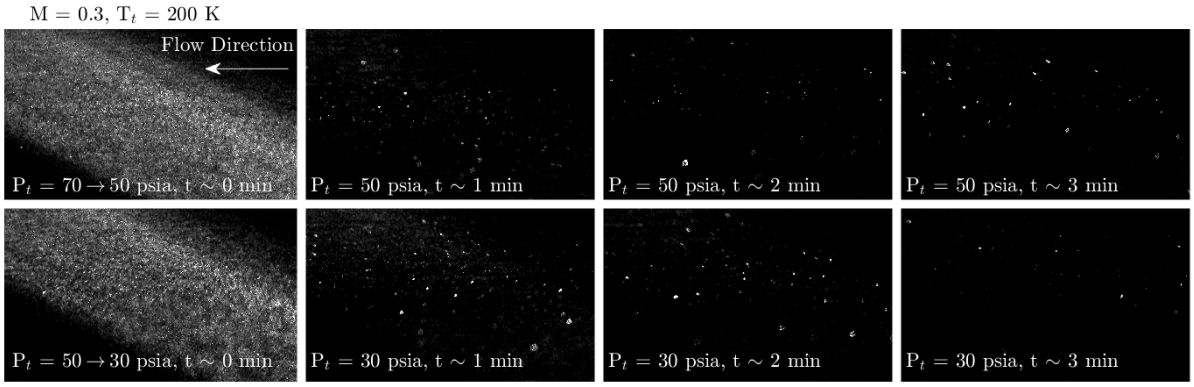

Fig. 7 Example droplet distributions as a function of time from pressure drops of 70 to 50 psia (top row) and 50 to 30 psia (bottom row). The tunnel total temperature and Mach number were fixed at 200 K and 0.3, respectively.

Once the tunnel was purged of air, the facility conditions were varied to look for LN_2 droplets. We wanted to induce a transient condition that produced adequate concentrations of droplets in the test section that remain while the tunnel returned to on-point conditions as defined by the facility operators. Starting at 300 K and dropping in increments of 20 K, the tunnel pressure was dropped from 70 to 50, and then 50 to 30 psia while looking for the onset of particles after each drop. No appreciable level of particles was observed until reaching T_t = 220 K, but even then, only minimal particles were observed. It wasn't until the temperature drop to 200 K that a significant number of particles appeared in the field-of-view of the detector. Once reaching 200 K, any pressure drops of ~20 psia consistently led to a large flux of LN_2 droplets that persisted in a usable level in the test section for several minutes as seen in Fig. 7. The initial drop is viewed on the first column, while the remaining columns represent acquisitions in roughly one-minute increments from the pressure drop and are when the facility is on-point. These trends continued to temperatures down to 160 K when tests were halted due to frost forming on the plenum window, and in general are consistent with previous observations presented earlier in Fig. 2.

C. Preliminary Results: Freestream PIV

As an initial check on the quality of these LN_2 droplets as flow tracers, the series of recorded image pairs like those from Fig. 7 minutes after the pressure drop were processed using the open source PIVlab code in MATLAB [69] and compared to the velocity results from the facility. The cross-correlation window sizes were 64x64 with a 32x32 final pass and an overlap of 50%. With this level and uniformity of seeding, the majority of the vectors were thrown out, but for this initial level of comparison and without control over the droplet density, the primary goal of this study was matching the velocities provided by the facility data acquisition system. Results for T_t = 160, 180, and 200 K are shown in Fig. 8 with the error bars listed as the standard deviation from single image pairs. Note that T_t = 140 K and 220 K were not examined because of the level of window frost and the overall lack of seeding, respectively. Even the 160 K case experiences higher deviations, due mostly to the frost on the window.

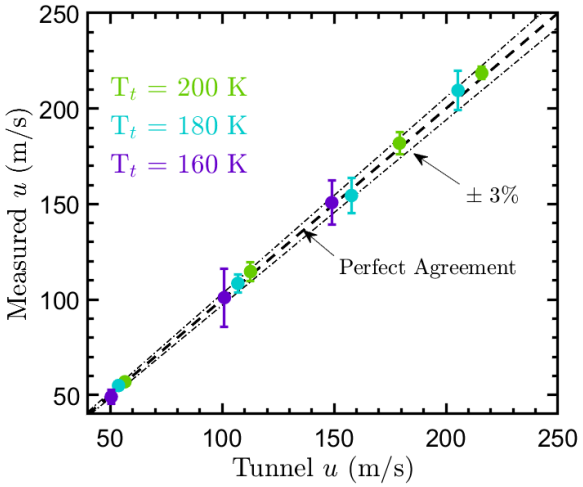

Fig. 8 Measured freestream velocity as a function of the set tunnel velocity to total temperatures of 200, 180, and 160 K.

On average, the measured mean velocities are within 1.5% of the facility freestream value, providing preliminary confirmation that these LN_2 particles accurately follow the flow. However, further investigations are required to determine the lag characters of these particles, as the measured freestream is essentially gradient-free.

D. Comparison of Processing Methods: PIV vs. PTV

Another area of open discussion in this proposed application is the appropriate post-processing scheme. We have demonstrated the ability to acquire time-resolved particle images in the 0.3-m TCT, but it remains unclear which post-processing algorithm would best produce the measured flowfield. For our case, without control over the particle size or concentration, use of both cross-correlation and particle tracking techniques may prove useful under certain conditions. To provide some preliminary insight into how these schemes may produce the final velocity fields, we looked at the output velocity vectors as a function of processing scheme from a time-resolved series of LN_2 droplet images recorded ~2 minutes after a pressure drop from 70 to 50 psia at T_t = 200 K and M = 0.2. The resulting vectors of single image pairs (top row) and the average of 100 image pairs (bottom row) for PIV cross-correlation schemes utilizing grid sizes of 32x32, 16x16, 8x8, and 4x4 and using a single PTV particle trajectory algorithm (far right side)

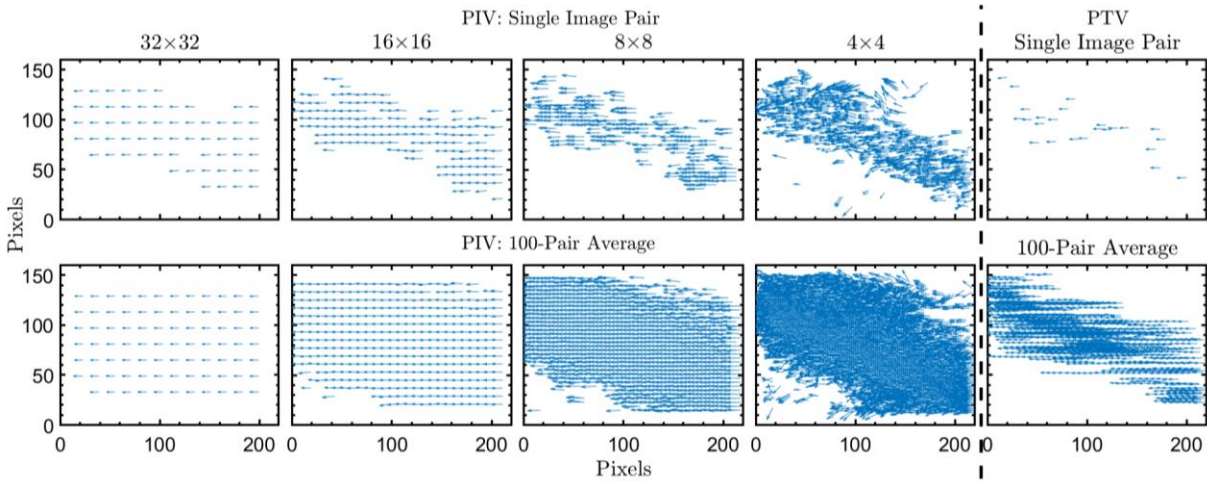

Fig. 9 Comparison of various correlation windows using PIV and PTV on the freestream flow. Single image pairs are shown on the top row, while the average over 100 images are shown on the bottom row.

are shown in Fig. 9. Both the PIV [69] and PTV [70] codes used were freely-available. All PIV processing steps included 3 passes, each with a 50% overlap with a single postprocessing step throwing out velocity vectors that are more than 2 standard deviations from the mean. The PTV algorithm simply used LN_2 trajectories from the time-resolved images to map out the flow, using a thresholding approach to identify particles based on size. Only particles consisting of 2 adjacent pixels with intensities above the selected threshold of 150 counts were used to determine a trajectory.

In general, all methods reproduce the velocity magnitude at this condition, but the spatial resolution and quality of vectors vary for PIV, where the finer the resolution, the worse the reproduced vector is in general. The flowfield in this freestream test case is overwhelmingly single-component, as is clearly seen with grid sizes of 32x32 down to 8x8 in Fig. 9, but a drop in correlation size to 4x4 results in several erroneous vectors. However, the PTV trajectory algorithm only produces velocity vectors for each droplet that passes through the field-of-view. Therefore, unlike PIV, where the resolution is predetermined by the grid size, the PTV resolution is dependent on the physical proximity of particles in the flow as seen with the single-image pairs in Fig. 9. This methodology leads to local regions of the flow having higher spatial resolutions than others, simply due to the particle distribution (i.e. the center of the PTV average image in Fig. 9 has many more trajectories than either end of the image). This trait alone may prove useful should the level of natural seeding decay, forcing us to "piece together" the average flowfield with trajectories from individual particles. It remains likely that both methods will be used for these LN_2 droplets in the future.

VI. Conclusions and Future Work

Unevaporated liquid nitrogen droplets have been observed in the test sections of the NASA Langley 0.3-m TCT and the NTF since their respective operational dates. Recent Rayleigh scattering instruments in both facilities helped characterize when these droplets occur and motivated a devoted effort to utilize these LN_2 droplets as the seed source for off-body velocimetry techniques. In this work, we have demonstrated accurate droplet-based velocimetry in the freestream flow of the 0.3-m TCT in the total temperature range of 160 to 200 K. This source of natural seeding, present in the flow to cool the test gas temperature and raise the Reynolds number, provides adequate levels of seed concertation to use PIV cross-correlation processing algorithms, while at times we may resort to PTV trajectory algorithms to locally increase the spatial resolution of the measured flowfield.

Significant future work is required to fully realize such an off-body velocimetry instrument in an engineering-relevant flow facility. Further droplet characterization is required, including size and lag measurements with respect to the otherwise gaseous flow. Confirmation of droplet flow-tracking must be acquired with separate measurements of the flow over a wing or cylindrical model. Finally, if proven successful in the 0.3-m TCT, this instrument will be applied to the much larger NTF facility.

Acknowledgments

The authors appreciate the assistance and expertise of the 0.3-m TCT facility staff, including Michael Chambers, Karl Maddox, Cliff Obara, Reggie Brown, and Tammy Price. Additional conversations with Eric Walker and Jim Meyers have been insightful. Josef Felver was supported by NASA SBIR Contract Number 80NSSC19C0612. The other researchers were supported by the Aerosciences Evaluation and Test Capabilities (AETC) Portfolio, Test Technology Focus Area under the leadership of James Bell and the ARMD TTT Innovative Measurements Discipline under the leadership of Tom Jones.

References

[1] Wegener, P. P. "Cryogenic Transonic Wind Tunnels and the Condensation of Nitrogen." *Experiments in Fluids*, Vol. 11, No. 5, 1991, pp. 333–338. https://doi.org/10.1007/BF00194865.

[2] Goodyer, M. J. "The Cryogenic Wind Tunnel." *Progress in Aerospace Sciences*, Vol. 29, No. 3, 1992, pp. 193–220. https://doi.org/10.1016/0376-0421(92)90008-6.

[3] Green, J., and Quest, J. "A Short History of the European Transonic Wind Tunnel ETW." *Progress in Aerospace Sciences*, Vol. 47, No. 5, 2011, pp. 319–368. https://doi.org/10.1016/j.paerosci.2011.06.002.

[4] Fuller, D. E. "Guide for Users of the National Transonic Facility." *NASA Technical Memorandum 83124*, 1981.

[5] Ray, E. J., Ladson, C. L., Adcock, J. B., Lawing, P. L., and Hall, R. M. "Review of Design and Operational Characteristics of the 0.3-Meter Transonic Cryogenic Tunnel." *NASA Technical Memorandum 80123*, 1979.

[6] Kilgore, R. A. "Design Features and Operational Characteristics of the Langley 0.3-Meter Transonic Cryogenic Tunnel." *NASA TN D-8304*, 1976.

[7] Michael, J. B., Edwards, M. R., Dogariu, A., and Miles, R. B. "Femtosecond Laser Electronic Excitation Tagging for Quantitative Velocity Imaging in Air." *Applied Optics*, Vol. 50, No. 26, 2011, pp. 5158–5162. https://doi.org/10.1364/AO.50.005158.

[8] Burns, R. A., Danehy, P. M., Halls, B. R., and Jiang, N. "Femtosecond Laser Electronic Excitation Tagging Velocimetry in a Transonic, Cryogenic Wind Tunnel." *AIAA Journal*, Vol. 55, No. 2, 2017, pp. 680–685. https://doi.org/10.2514/1.J055325.

[9] Burns, R. A., and Danehy, P. M. "Unseeded Velocity Measurements around a Transonic Airfoil Using Femtosecond Laser Tagging." *AIAA Journal*, Vol. 55, No. 12, 2017, pp. 4142–4154. https://doi.org/10.2514/1.J056154.

[10] Burns, R. A., Peters, C. J., and Danehy, P. M. "Unseeded Velocimetry in Nitrogen for High-Pressure, Cryogenic Wind Tunnels, Part I: Femtosecond-Laser Tagging." *Measurement Science and Technology*, Vol. 29, No. 115302, 2018. https://doi.org/10.1088/1361-6501/aade1b.

[11] Burns, R. A., Danehy, P. M., Jiang, N., Slipchenko, M. N., Felver, J., and Roy, S. "Unseeded Velocimetry in Nitrogen for High-Pressure, Cryogenic Wind Tunnels, Part II: Picosecond-Laser Tagging." *Measurement Science and Technology*, Vol. 29, No. 115203, 2018. https://doi.org/10.1088/1361-6501/aade1b.

[12] Reese, D., Danehy, P., Jiang, N., Felver, J., Richardson, D., and Gord, J. "Application of Resonant Femtosecond Tagging Velocimetry in the 0.3-Meter Transonic Cryogenic Tunnel." *AIAA Journal*, Vol. 57, No. 9, 2019, pp. 3851–3858. https://doi.org/10.2514/1.J057981.

[13] Reese, D. T., Jiang, N., and Danehy, P. "Unseeded Velocimetry in Nitrogen for High-Pressure, Cryogenic Wind Tunnels: Part III. Resonant Femtosecond-Laser Tagging." *Measurement Science and Technology*, Vol. 31, No. 7, 2020, pp. 1–15. https://doi.org/https://doi.org/10.1088/1361-6501/ab7bbc.

[14] Reese, D., Burns, R. A., Danehy, P. M., Walker, E., and Goad, W. *Implementation of a Pulsed-Laser Measurement System in the National Transonic Facility*. AIAA Aviation 2019 Forum, 2019.

[15] Reese, D., Danehy, P. M., Walker, E. L., Rivers, M. B., and Goad, W. K. *FLEET Velocimetry in the Common Research Model's Wing Wake*. AIAA Scitech 2020 Forum, 2020.

[16] Danehy, P. M., Bathel, B. F., Calvert, N., Dogariu, A., and Miles, R. P. *Three-Component Velocity and Acceleration Measurement Using FLEET*. 30th AIAA Aerodynamic Measurement Technology and Ground Testing Conference, 2014.

[17] Willert, C., Stockhausen, G., Beversdorff, M., Klinner, J., Lempereur, C., Barricau, P., Quest, J., and Jansen, U. "Application of Doppler Global Velocimetry in Cryogenic Wind Tunnels." *Experiments in Fluids*, Vol. 39, No. 2, 2005, pp. 420–430. https://doi.org/10.1007/s00348-004-0914-z.

[18] Richard, H., Becker, W., Loose, S., Thimm, M., Bosbach, J., and Raffel, M. *Application of Particle Image Velocimetry under Cryogenic Conditions*. ICIASF Record, International Congress on Instrumentation in Aerospace Simulation Facilities, 2003.

[19] Konrath, R., Otter, D., Geisler, R., Agocs, J., Mattner, H., Roosenboom, E. W. M., Fey, U., Quest, J., and Kühn, C. *Adaptation of PIV for Application in Cryogenic Pressurized Wind Tunnel Facilities at High Reynolds Numbers*. 15th Int. Symp. on Applications of Laser Techniques to Fluid Mechanics, 2010.

[20] Quest, J., and Konrath, R. *Accepting a Challenge - The Development of PIV for Application in Pressurized Cryogenic Wind Tunnels*. 41st AIAA Fluid Dynamics Conference and Exhibit, 2011.

[21] Konrath, R., Agocs, J., Geisler, R., Otter, D., Roosenboom, E. W. M., Wolf, T., and Quest, J. *Flow Field Measurements by PIV at High Reynolds Numbers*. 51st AIAA Aerospace Sciences Meeting including the New Horizons Forum and Aerospace Exposition, 2013.

[22] Konrath, R., Geisler, R., Agocs, J., Otter, D., Ehlers, H., Philipp, F., and Quest, J. *Tracking the Nacelle Vortex above Aircraft Wing in the ETW at Real Mach- and Reynolds Numbers by Means of PIV*. 53rd AIAA Aerospace Sciences Meeting, 2015.

[23] Gloss, B., and Bruce, R. *A Solution to Water Vapor in the National Transonic Facility*. 27th Aerospace Sciences Meeting, 1989.

[24] Reeder, M. F., Crafton, J. W., Estevadeordal, J., Delapp, J., McNiel, C., Peltier, D., and Reynolds, T. "Clean Seeding for Flow Visualization and Velocimetry Measurements." *Experiments in Fluids*, Vol. 48, No. 5, 2010, pp. 889–900. https://doi.org/10.1007/s00348-009-0784-5.

[25] Melling, A. "Tracer Particles and Seeding for Particle Image Velocimetry." *Measurement Science and Technology*, Vol. 8, No. 12, 1997, pp. 1406–1416. https://doi.org/10.1088/0957-0233/8/12/005.

[26] Ruan, Y., Chen, L., Liu, X., Chen, S., and Hou, Y. "Numerical Study of Evaporation and Motion Characteristics of Liquid Nitrogen Droplet in High-Speed Gas Flow." *IOP Conference Series: Materials Science and Engineering*, Vol. 278, 2017. https://doi.org/10.1088/1757-899X/278/1/012130.

[27] Hall, R. M., and Kramer, S. A. "A Review of at Rest Droplet Growth Equations for Condensing Nitrogen in Transonic Cryogenic Wind Tunnels." *NASA Technical Memorandum 78821*, 1979.

[28] Hall, R. *Condensation and Its Growth down the Test-Section of the Langley 0.3-m Transonic Cryogenic Tunnel*. 10th Aerodynamic Testing Conference, 1978.

[29] Hall, R. M. "Onset of Condensation Effects with an NACA 0012-64 Airfoil Tested in the Langley 0.3-Meter Transonic Cryogenic Tunnel." *NASA Technical Paper 1385*, 1979.

[30] Hall, R. M. *Pre-Existing Seed Particles and the Onset of Condensation in Cryogenic Wind Tunnels.* AIAA 22nd Aerospace Sciences Meeting, 1984.

[31] Aguilar, G., Majaron, B., Verkruysse, W., Zhou, Y., Nelson, J. S., and Lavernia, E. J. "Theoretical and Experimental Analysis of Droplet Diameter, Temperature, and Evaporation Rate Evolution in Cryogenic Sprays." *International Journal of Heat and Mass Transfer*, Vol. 44, No. 17, 2001, pp. 3201–3211. https://doi.org/10.1016/S0017-9310(00)00363-X.

[32] Franco, W., Vu, H., Jia, W., Stuart Nelson, J., and Aguilar, G. "Fluid and Thermal Dynamics of Cryogen Sprays Impinging

on a Human Tissue Phantom." *Journal of Biomechanical Engineering*, Vol. 130, No. 5, 2008, pp. 1–21. https://doi.org/10.1038/jid.2014.371.

[33] Ingebo, R. "Atomizing-Gas Temperature Effect on Cryogenic Spray Dropsize." *NASA Technical Memorandum 106106*, 1993.

[34] Ingebo, R. D. *Characteristics of Vaporizing Cryogenic Sprays for Rocket Combustion Modeling*. NASA Technical Memorandum 106615, 1994.

[35] Rees, A., Araneo, L., Salzmann, H., Kurudzija, E., Suslov, D., Sender, J., and Oschwald, M. *Investigation of Velocity and Droplet Size Distributions of Flash Boiling LN2-Jets With Phase Doppler Anemometry*. 29th Conference on Liquid Atomization and Spray Systems, 2019.

[36] Luo, M., Wu, Y., and Haidn, O. J. "Temperature and Size Measurements of Cryogenic Spray Droplets with Global Rainbow Refractometry." *Journal of Propulsion and Power*, Vol. 35, No. 2, 2019, pp. 359–368. https://doi.org/10.2514/1.B36750.

[37] Phillips, D. R., Smith, E. A., and Suomi, V. E. An Automated Technique for Obtaining Cloud Motion From Geosynchronous Satellite Data Using Cross Correlation. *Journal of Applied Meteorology*. 4. Volume 11, 752–754.

[38] Emery, W. J., Fowler, C. W., Hawkins, J., and Preller, R. H. "Fram Strait Satellite Image-Derived Ice Motions." *Journal of Geophysical Research*, Vol. 96, No. C3, 1991, pp. 4751–4768. https://doi.org/10.1029/90JC02273.

[39] Muste, M., Fujita, I., and Hauet, A. "Large-Scale Particle Image Velocimetry for Measurements in Riverine Environments." *Water Resources Research*, Vol. 46, No. 4, 2008, pp. 1–14. https://doi.org/10.1029/2008WR006950.

[40] Kim, Y. *Uncertainty Analysis for Non-Intrusive Measurement of River Discharge Using Image Velocimetry*. PhD Thesis, 2006.

[41] Holland, K. T., Puleo, J. A., and Kooney, T. N. "Quantification of Swash Flows Using Video-Based Particle Image Velocimetry." *Coastal Engineering*, Vol. 44, No. 2, 2001, pp. 65–77. https://doi.org/10.1016/S0378-3839(01)00022-9.

[42] Toloui, M., Riley, S., Hong, J., Howard, K., Chamorro, L. P., Guala, M., and Tucker, J. "Measurement of Atmospheric Boundary Layer Based on Super-Large-Scale Particle Image Velocimetry Using Natural Snowfall." *Experiments in Fluids*, Vol. 55, No. 5, 2014, pp. 1–14. https://doi.org/10.1007/s00348-014-1737-1.

[43] Politz, C., Lawson, N. J., Konrath, R., Agocs, J., and Schroder, A. Development of Particle Image Velocimetry for In-Flight Flow Measurements. In *Advanced In-Flight Measurement Techniques*, 2013, pp. 269–289.

[44] Choi, S. M., Kim, W. H., Côté, D., Park, C.-W., and Lee, H. "Blood Cell Assisted in Vivo Particle Image Velocimetry Using the Confocal Laser Scanning Microscope." *Optics Express*, Vol. 19, No. 5, 2011, p. 4357. https://doi.org/10.1364/oe.19.004357.

[45] Bitsch, L., Olesen, L. H., Westergaard, C. H., Bruus, H., Klank, H., and Kutter, J. P. "Micro Particle-Image Velocimetry of Bead Suspensions and Blood Flows." *Experiments in Fluids*, Vol. 39, No. 3, 2005, pp. 505–511. https://doi.org/10.1007/s00348-005-0967-7.

[46] Rose, W. C., and Johnson, D. A. "Turbulence in a Shock-Wave Boundary-Layer Interaction." *AIAA Journal*, Vol. 13, No. 7, 1975, pp. 884–889. https://doi.org/10.2514/3.60464.

[47] Johnson, D. A., and Rose, W. C. "Laser Velocimeter and Hot-Wire Anemometer Comparison in a Supersonic Boundary Layer." *AIAA Journal*, Vol. 13, No. 4, 1975, pp. 512–515. https://doi.org/10.2514/3.49739.

[48] Reinath, M. S. "Laser Velocimeter for Large Wind Tunnels." *Journal of Aircraft*, Vol. 19, No. 12, 1982, pp. 1100–1102. https://doi.org/10.2514/3.44820.

[49] Owen, F. K. "Application of Laser Velocimetry to Unsteady Flows in Large Scale High Speed Tunnels." *NASA-CR-166575*, 1983.

[50] Kirmse, T., Agocs, J., Schröder, A., Schramm, M. J., Karl, S., and Hannemann, K. "Application of Particle Image Velocimetry and the Background-Oriented Schlieren Technique in the High-Enthalpy Shock Tunnel Göttingen." *Shock Waves*, Vol. 21, No. 3, 2011, pp. 233–241. https://doi.org/10.1007/s00193-011-0314-2.

[51] Zhang, W., Wang, Y., and Lee, S. J. "Simultaneous PIV and PTV Measurements of Wind and Sand Particle Velocities." *Experiments in Fluids*, Vol. 45, No. 2, 2008, pp. 241–256. https://doi.org/10.1007/s00348-008-0474-8.

[52] Kilgore, R. A. "Design Features and Operational Characteristics of the Langley Pilot Transonic Cryogenic Tunnel." *NASA TM X-72012*, 1974.

[53] Mineck, R. E. "Hardware and Operating Features of the Adaptive Wall Test Section for the Langley 0.3-Meter Transoic Cryogenic Tunnel." *NASA Technical Memorandum 4114*, 1989.

[54] Gartrell, L. R., Gooderum, P. B., Hunter Jr., W. W., and Meyers, J. F. "Laser Velocimetry Technique Applied to the Langley 0.3-Meter Transonic Cryogenic Tunnel." *NASA Technical Memorandum 81913*, 1981.

[55] Honaker, W. C. "Velocity and Flow Angle Measurements in the Langley 0.3-Meter Transonic Cryogenic Tunnel Using a Laser Transit Anemometer." *NASA-CP2243*, 1982.

[56] Singh, J. J., Marple, C. G., and Davis, W. T. "Characterization of Particles in the Langley 0.3-Meter Transonic Cryogenic Tunnel Using Hot Wire Anemometry." *NASA Technical Memorandum 84551*, 1982.

[57] Honaker, W. C., and Lawing, P. L. "Measurements in the Flow Field of a Cylinder with a Laser Transit Anemometer and a Drag Rake in the Langley 0.3 M Transonic Cryogenic Tunnel." *NASA Technical Memorandum 86399*, 1985.

[58] Selby, G. V. *Vapor-Screen Flow-Visualization Experiments in the NASA Langley 0.3-M Transonic Cryogenic Tunnel.* NASA Contractor Report 3984, 1986.

[59] Lawing, P. L., Johnson, C. B., Beach, W. P., Tunnel, T. C., Lawing, L., and Johnson, C. B. *Summary of Test Techniques Used in the NASA-Langley 0.3m Transonic Cryogenic Tunnel*. AIAA 14th Aerodynamic Testing Conference, 1986.

[60] Shirinzadeh, B., Herring, G. C., and Barros, T. "Demonstration of Imaging Flow Diagnostics Using Rayleigh Scattering in Langley 0.3-Meter Transonic Cryogenic Tunnel." *NASA Technical Memorandum 1999-208970*, 1999.

[61] Herring, G. C., and Shirinzadeh, B. "Flow Visualization of Density in a Cryogenic Wind Tunnel Using Planar Rayleigh and Raman Scattering." *NASA Technical Memorandum 2002-211630*, 2002.

[62] Burns, R. A., Peters, C. J., and Danehy, P. M. "Unseeded Velocimetry in Nitrogen for High-Pressure, Cryogenic Wind Tunnels, Part I: Femtosecond-Laser Tagging." *Measurement Science and Technology*, Vol. 29, No. 11, 2018. https://doi.org/10.1088/1361-6501/aade1b.

[63] Burns, R. A., and Danehy, P. M. *Rayleigh Scattering Density Measurements from Ultrafast Lasers in High-Pressure, Cryogenic Wind Tunnels*. 2018 AIAA Aerospace Sciences Meeting, 2018.

[64] Thibodeaux, J. J., and Balakrishna, S. "Automatic Control of a 0.3 m Cryogenic Test Facility." *Journal of Guidance, Control, and Dynamics*, Vol. 4, No. 4, 1980, pp. 428–432. https://doi.org/10.2514/3.56095.

[65] Kilgore, R. A., Igoe, W. B., Adcock, J. B., Hall, R. M., Johnson, C. B., and Si, N. I. "Full-Scale Aircraft Simulation with Cryogenic Tunnels and Status of the National Transonic Facility." *NASA TM-80085*, 1979.

[66] Hunter Jr, W. W., Gartrell, L. R., and Honaker, W. C. "Some NTF Laser Velocimeter Installation and Operation Considerations." *NASA-CP2243*, 1982.

[67] Herring, G. C., Lee, J. W., and Goad, W. K. "Feasibility of Rayleigh Scattering Flow Diagnostics in the National Transonic Facility." *NASA Technical Memorandum 2015-218800*, 2015.

[68] Crouch, J. D., Sutanto, M. I., Witkowski, D. P., Watkins, A. N., Rivers, M. B., and Campbell, R. L. *Assessment of the National Transonic Facility for Laminar Flow Testing*. 48th AIAA Aerospace Sciences Meeting Including the New Horizons Forum and Aerospace Exposition, 2010.

[69] Thielicke, W., and Stamhuis, E. J. "PIVlab – Towards User-Friendly, Affordable and Accurate Digital Particle Image Velocimetry in MATLAB." *Journal of Open Research Software*, Vol. 2, 2014. https://doi.org/10.5334/jors.bl.

[70] Janke, T., Schwarze, R., and Bauer, K. "Part2Track: A MATLAB Package for Double Frame and Time Resolved Particle Tracking Velocimetry." *SoftwareX*, Vol. 11, 2020, p. 100413. https://doi.org/10.1016/j.softx.2020.100413.